Variable-range hopping conductivity and structure of density of localized states in $LaMnO_{3+\delta}$ under pressure

2006 J. Phys.: Condens. Matter 18 10291

(http://iopscience.iop.org/0953-8984/18/45/015)

INSTITUTE OF PHYSICS PUBLISHING JOURNAL OF PHYSICS: CONDENSED MATTER

J. Phys.: Condens. Matter **18** (2006) 10291–10302 doi:10.1088/0953-8984/18/45/015

Variable-range hopping conductivity and structure of density of localized states in $LaMnO_{3+\delta}$ under pressure

R Laiho[1], K G Lisunov[1,2], E Lähderanta[3], M L Shubnikov[1,4], Yu P Stepanov[1,4], P A Petrenko[2], A Khokhulin[5] and V S Zakhvalinskii[1,5]

[1] Wihuri Physical Laboratory, University of Turku, FIN-20014 Turku, Finland
[2] Institute of Applied Physics, Academiei Street, 5, MD-2028 Kishinev, Moldova
[3] Department of Physics, Lappeenranta University of Technology, PO Box 20, FIN-53851 Lappeenranta, Finland
[4] A F Ioffe Physico-Technical Institute, 194021 St Petersburg, Russia
[5] Belgorod State University, Pobeda Street 85, 308015 Belgorod, Russia

Received 30 May 2006, in final form 19 September 2006
Published 27 October 2006
Online at stacks.iop.org/JPhysCM/18/10291

Abstract

The temperature dependence of the resistivity, ρ, of ceramic $LaMnO_{3+\delta}$ with $\delta = 0.065$ and 0.154 (or simply # 065 and # 154), is investigated under hydrostatic pressure, p, between the temperatures $T = 80$ and 320 K in magnetic fields up to 10 T. The data for $\rho(T)$ are analysed within a Shklovskii–Efros-like variable-range hopping conductivity model, governed by a soft Coulomb gap, Δ, and a rigid gap, γ, in the density of localized states. The validity of this approach to the resistivity of $LaMnO_{3+\delta}$ under ambient pressure was established in recent investigations (Laiho *et al* 2005 *J. Phys: Condens. Matter* **17**, 105). In the present work it is shown that upon increasing p up to 11 kbar (# 154) and 13 kbar (# 065) the magnetic Curie temperature, T_C, is increased by ∼12–13%. Correspondingly, $\Delta(p)$ is decreased by ∼7–8% and $\gamma(p)$ by ∼8% in # 154 and 12% in # 065. Similarly, the electron localization radius $a(p)$ is increased by ∼4% in # 154 and 8% in # 065, respectively. The influence of pressure on T_C, Δ, γ and a is interpreted by increasing the electron bandwidth and decreasing the polaron potential well, which stimulates the delocalization of electrons when p is increased.

(Some figures in this article are in colour only in the electronic version)

1. Introduction

Non-stoichiometric $LaMnO_{3+\delta}$ belongs to the group of hole-doped mixed-valence manganite perovskites $La_{1-x}A_xMnO_3$, demonstrating colossal magnetoresistance (CMR) near the paramagnetic (PM) to ferromagnetic (FM) transition temperature, T_C [1, 2]. Hole doping in these materials is usually obtained by substitution of a divalent alkaline element A (Ca, Ba, Sr, etc) for trivalent La. This leads to mixed valence ions $Mn^{3+,4+}$ and Mn^{3+}–Mn^{4+} pairs coupled

with ferromagnetic double-exchange (DE) interaction [2, 3]. The relative concentration of the holes, c, given by the Mn^{4+}/Mn^{3+} ratio, is close to x when the contribution of lattice defects is small. On the other hand, because excess oxygen cannot occupy interstitial sites in the perovskite structure, hole doping of $LaMnO_{3+\delta}$ is possible only by the creation of lattice defects connected to cation vacancies with concentration $\delta' = (2/3)\delta$ corresponding to $c = 2\delta$ [4].

The electronic properties of the manganite perovskites above T_C are governed by electron localization presumably due to strong electron–phonon interaction and the local Jahn–Teller distortions leading to the formation of a small-polaron state [2, 5]. Nearest-neighbour hopping (NNH) conductivity of the small polarons satisfying the Arrhenius law is observed above room temperature, e.g. in $La_{1-x}Ca_xMnO_3$ up to $T \sim 1200$ K [6]. However, on lowering the temperature a transition to variable-range hopping (VRH) conductivity is observed. Generally, VRH is strongly influenced by details of the density, $g(\varepsilon)$, of localized states (DOS), such as a *soft* Coulomb gap, Δ, and a *rigid* gap, γ, around the Fermi level, μ [7, 8]. The term soft gap means that $g(\varepsilon)$ decreases parabolically when ε tends to μ and vanishes at $\varepsilon = \mu$, whereas the term rigid gap (sometimes named as hard gap) means a finite interval $(\mu - \gamma, \mu + \gamma)$ where $g(\varepsilon) = 0$. Existence of these gaps has been established in scanning-tunnelling spectroscopy investigations of CMR perovskite $La_{0.8}Ca_{0.2}MnO_3$ films (giving $\Delta \sim 0.5$ eV and temperature-dependent γ up to ~0.11 eV) [9] and in transport and optical investigations of non-CMR perovskite $SrTi_{1-x}Ru_xO_3$ films [10]. Effects connected to Δ and γ were observed also in the VRH conductivity of various non-perovskite materials, such as amorphous $Si_{1-x}Mn_x$ [11] and In/InO_x [12] films, as well as in $Cd_{0.91}Mn_{0.09}Te$:In [13] and β-$FeSi_2$ [14] single crystals.

Therefore, investigations of VRH conductivity are useful for determination of the DOS features and other microscopic parameters such as the localization radius, a, of hopping charge carriers. Namely, in $La_{0.7}Ca_{0.3}Mn_{1-y}Fe_yO_3$ ($y = 0$–0.09) the Shklovskii–Efros-like VRH conductivity law, $\ln \rho \sim T^{-1/2}$ [7], has been observed below the onset temperature $T_v \approx 310$–330 K, yielding $\Delta \approx 0.40$–0.44 eV and a temperature-dependent rigid gap $\gamma(T) \approx \gamma_v(T/T_v)^{1/2}$, where $\gamma_v \equiv \gamma(T_v) \approx 0.16$–$0.12$ eV and $a \approx 2.5$–2.9 Å, respectively [8]. For $La_{1-x}Ba_xMnO_3$ ($x = 0.02$–0.10) the values of $T_v = 250$–280 K, $\Delta \approx 0.44$–0.46 eV, $\gamma_v \approx 0.14$–0.18 eV and $a \approx 2.0$–2.4 Å, respectively, have been reported [15]. In $LaMnO_{3+\delta}$ ($\delta = 0.100$–0.154) with $T_v \approx 250$–270 K the value of $\Delta \approx 0.43$–0.48 eV is close to those above, and those of $\gamma_v \approx 0.13$–0.17 eV (increasing with δ) and $a \approx 1.7$–1.2 Å (decreasing with δ) correlate well with progressive lattice distortions when δ is increased [16].

All the values of a cited above are smaller than the mean distance, R, between the Mn sites, satisfying the requirement for small-polaron formation [17]. In addition, the values of the effective dielectric constant $\kappa \approx 3.4$ and 3.5 found from the analysis of the VRH conductivity in $La_{0.7}Ca_{0.3}Mn_{1-y}Fe_yO_3$ [8] and $LaMnO_{3+\delta}$ [16], respectively, are much smaller than the static dielectric permittivity $\kappa_0 \sim 20$ of the manganite perovskites [18] and close to $\kappa_p = (\kappa_\infty^{-1} - \kappa_0^{-1})^{-1} \sim 4$–$5$ [18]. In $La_{1-x}Ba_xMnO_3$ the values of $\kappa \approx 3.2$–3.4 and $\kappa_p \approx 3.3$–5.3, obtained independently from VRH conductivity in a wide temperature range [15], agree with each other and are similar to the values of κ_p above. Therefore, the values of Δ, a and κ in perovskites are consistent with the VRH model of small polarons with mutual Coulomb repulsions, where $\Delta \sim U \approx e^2/(\kappa_p R)$ is a typical electrostatic interaction energy between the polarons on nearest sites [17]. Hence, the origin of the rigid gap γ in perovskites may be associated with polaron formation, too. Namely, to hop from a site with energy below μ to another site with energy above μ, the electron should annihilate the polarization of the medium on the initial site and create it on the final site [17]. This requires a minimum hopping energy leading to the appearance of a rigid gap in the DOS around μ if the polarization of the lattice and the surrounding spins are more important for localization of the electrons than the lattice and spin disorder.

In this paper we investigate the resistivity, $\rho(T)$, of $LaMnO_{3+\delta}$ under hydrostatic pressure to obtain information about the microscopic parameters Δ, γ_v and a. This method provides a way for the determination of the rigid gap in the manganite perovskites that is independent of the methods used previously [8, 9, 15, 16].

2. Experimental details

Ceramic $LaMnO_{3+\delta}$ samples were prepared with the standard solid-state reaction method, combining argon and oxygen treatments with annealing in air (for details see [16] and [19]). The values of δ were determined by gravimetric and iodometric titration methods [19, 20]. Using room-temperature x-ray diffraction investigations the $LaMnO_{3+\delta}$ samples were divided into three groups characterized by (i) the orthorhombic $Pbnm$ structure with lattice parameters $a = 5.531(1)$ Å, $b = 5.536(1)$ Å and $c = 7.689(2)$ Å for $\delta = 0$, (ii) the cubic $Pm3m$ structure with small rhombohedral distortions and lattice parameter decreasing between $a = 7.813(2)$ and 7.791(1) Å when δ is increased from 0.065 to 0.112, and (iii) the rhombohedral $R\bar{3}c$ structure with lattice parameters decreasing in the intervals of $a = 5.530(2)$–$5.516(1)$ Å and $c = 13.333(5)$–$13.311(4)$ Å when δ varies between 0.125 and 0.154 [16, 19].

At ambient pressure the magnetoresistance (MR) of the sample with $\delta = 0$ is negligible, which is connected to the absence of Mn^{4+}. The hole-doped samples with δ between 0.065 and 0.154 exhibit the CMR effect [15]. Therefore, for measurements of $\rho(T)$ under pressure the group (ii) sample with $\delta = 0.065$ (labelled as # 065) and the group (iii) sample with $\delta = 0.154$ (labelled as # 154) were chosen. Magnetization measurements at $p = 1$ bar yielded the values of $T_C \approx 150$ K for # 065 and 135 K for # 154 [19].

Investigations of $\rho(T)$ were made using the four-probe technique. Hydrostatic pressure, p, up to 11 kbar for # 154 and up to 13 kbar for # 065, was applied using a Be–Cu cell with petrol–oil pressure transmitting fluid. For # 065 the values of $\rho(T)$ were measured at different pressures in magnetic fields up to 10 T.

3. Results and analysis

As can be concluded from figure 1, $\rho(T)$ at ambient pressure and $B = 0$ has activated character both above and below T_C, exhibits a weak inflection around T_C (shown by open triangles) and decreases with δ, in agreement with previous results [16]. When p is increased the resistivity decreases, exhibiting a stronger pressure effect for # 065 and exponential temperature dependence of the conductivity. The MR of # 154 at ambient pressure was investigated previously [16]. Typical plots of the MR of # 065 (inset of figure 1 for $p = 5$ kbar) exhibit activated behaviour at all B, too. In addition, the CMR effect is evident near the inflection of $\rho(T)$ at $B = 0$. This inflection, however, disappears when B is increased, as is characteristic of the PM–FM transition.

Detailed analysis of the resistivity in $LaMnO_{3+\delta}$ with $\delta = 0.100$–0.154 at ambient pressure [16] has demonstrated that $\rho(T)$, between $T_v = 250$–270 K and $T_C = 135$–162 K (depending on δ), obeys the Shklovskii–Efros-like VRH conductivity law [7],

$$\rho(T) = \rho_0(T) \exp[(T_0/T)^{1/2}], \tag{1}$$

where the prefactor has the form $\rho_0(T) = AT^{9/2}$ and the parameters A and T_0 do not depend on T [16]. In addition, A fits well the law

$$A = Ca^{11}T_0^{7/2}, \tag{2}$$

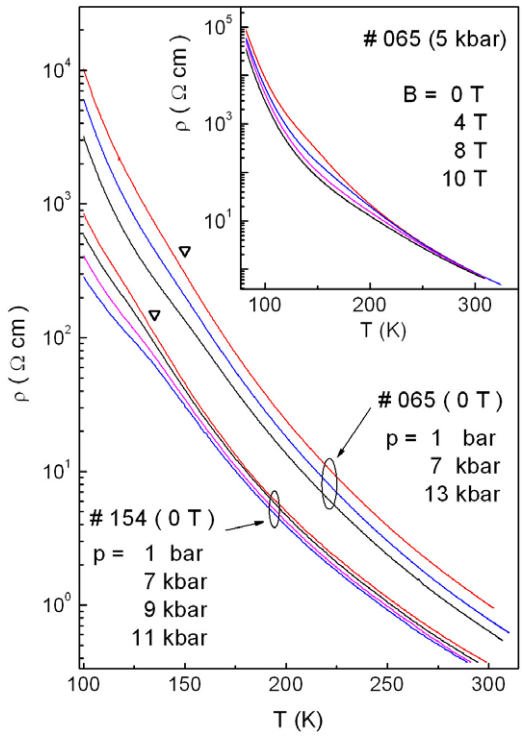

Figure 1. Temperature dependence of the resistivity in # 065 and # 154 under pressure increasing from top to bottom. The open triangles mark T_C at ambient pressure [14]. Inset: temperature dependence of the resistivity in # 065 at $p = 5$ kbar in magnetic field increasing from top to bottom.

where C is a constant, and the characteristic temperature T_0 satisfies the equation

$$T_0 = \left(\frac{\gamma_v}{2k\sqrt{T_v}} + \sqrt{\frac{\gamma_v^2}{4k^2 T_v} + T_{0SE}} \right)^2 \tag{3}$$

with the Shklovskii–Efros characteristic temperature $T_{0SE} = \beta e^2/(\kappa k a)$ and $\beta = 2.8$ [10]. Equations (1)–(3), describing all the features of the VRH conductivity also in other CMR materials [8, 15] (see section 1), have been obtained by taking into account the soft (Δ) and the rigid (γ) gaps in the DOS near the Fermi level [8].

Therefore, our analysis of $\rho(T)$ in # 065 and # 154 under applied pressure (figure 1) is based on equations (1)–(3). Below we will also use two other equations following from the model in [8], which connect Δ and γ_v to the temperature parameters T_0 and T_v and the DOS outside the Coulomb gap, g_0,

$$\Delta \approx k(T_0 T_v)^{1/2} \qquad \text{and} \qquad g_0 \approx (3/\pi)(\kappa^3/e^6)(\Delta - \gamma_v)^2. \tag{4}$$

It is evident from figure 2 that the plots of $\ln[\rho(T)/T^{9/2}]$ versus $T^{-1/2}$ are linear below the onset temperature T_v, whereas deviations from linearity on lowering T are observed only for $T \to T_C$ ($T_C^{-1/2}$ is marked with open triangles for $p = 1$ bar). The values of $T_v(p)$, $T_0(p)$ and $A(p)$ obtained from the linear parts of these plots are shown in figure 3 (all symbols with asterisks, e.g. T_v^*, etc, correspond to $p = 1$ bar and are collected in table 1). The values of $\Delta(p)$ evaluated with the first of equations (4) are displayed in figure 4. The relative variation

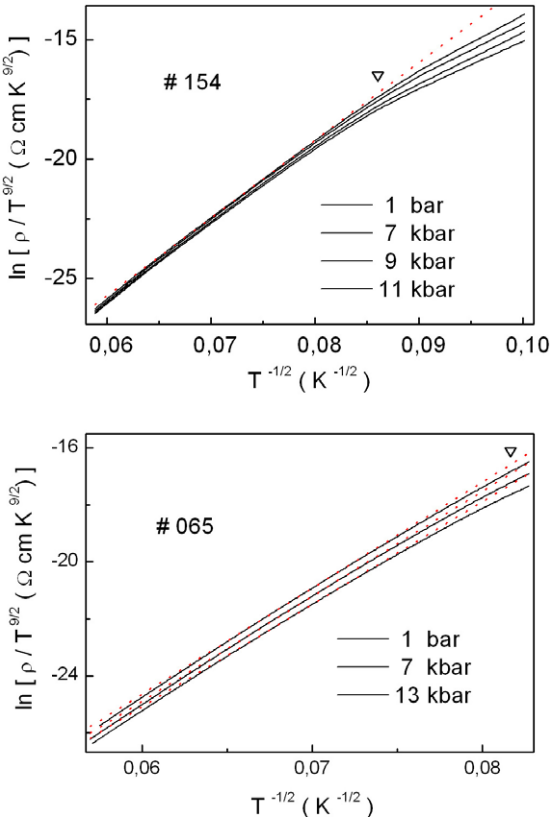

Figure 2. The plots of $\ln(\rho/T^{9/2})$ versus $T^{-1/2}$ for # 143 (top panel) and # 065 (bottom panel) under pressure increasing from top to bottom. The dotted lines are linear fits (for # 154 only at $p = 1$ bar) and the open triangles mark $T_C^{-1/2}$ obtained from magnetization measurements [14].

Table 1. The values of the Curie temperature T_C^*, the onset VRH temperature T_v^*, the characteristic temperature T_0^*, the prefactor constant A^*, the width of the Coulomb gap Δ^*, the localization radius a^* and the width of the rigid gap γ_v^* at ambient pressure, and the values of the effective dielectric constant κ, the baric coefficients dT_C/dp and $d\ln T_C/dp$ for the investigated $LaMnO_{3+\delta}$ samples.

Sample	T_C^* (K)	T_v^* (K)	T_0^* (10^5 K)	A^* (10^{-20} Ω cm $K^{-9/2}$)	Δ^* (eV)	a^* (Å)	γ_v^* (eV)	κ	dT_C/dp (K $kbar^{-1}$)	$d\ln T_C/dp$ (10^{-3} $kbar^{-1}$)
# 065	147	240	1.40	3.37	0.50	2.4	0.28	3.0	1.38 ± 0.03	8.9 ± 0.2
# 154	129	280	1.06	2.18	0.47	1.7	0.14	3.7	2.3 ± 0.2	16 ± 2

of the localization radius, $a(p)/a^*$, is obtained with equation (2) using the data for $A(p)$ and $T_0(p)$, and is shown with closed triangles in figure 5.

For further analysis we determine the values of $T_C(p)$ from the inflection points of $\rho(T)$ for given value of p and $B = 0$. The values of T_C^* collected in table 1 are close to those obtained in both samples from the magnetization data at ambient pressure [19] (see section 2). The pressure dependences of $T_C(p)/T_C^*$ in the inset to the bottom panel of figure 3 are close to linear, although in # 154 the onset of the linear behaviour is shifted to $p \sim 5$ kbar. The values of the baric coefficients dT_C/dp and $d(\ln T_C)/dp$ are given in table 1.

As can be seen from equations (2)–(4) the macroscopic parameters T_0, T_v and A, and the microscopic parameters Δ, γ_v, g_0 and a are interrelated. Therefore, we analyse quantitatively

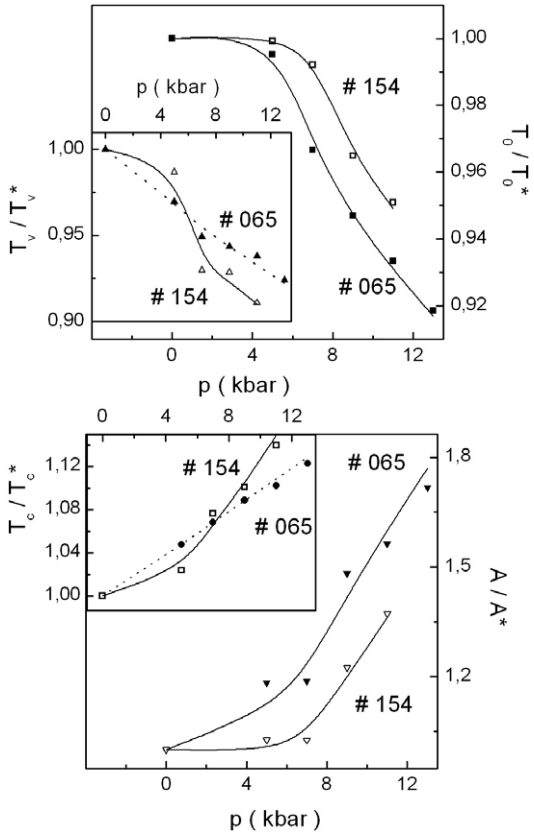

Figure 3. Pressure dependences of T_0/T_0^*, T_v/T_v^* (top panel) and A/A^*, T_C/T_C^* for # 064 and # 154. The lines are to guide the eye.

only the dependence of Δ on p using the second of equations (4) to get

$$\Delta(p) \approx \gamma_v(p) + (\pi/3)^{1/2} e^3 g_0^{1/2}(p)/(\kappa^{3/2}), \tag{5}$$

and from equation (3)

$$\gamma_v(p) = k[T_v(p)/T_0(p)]^{1/2}\{T_0(p) - \beta e^2/[\kappa k a^* a(p)/a^*]\}. \tag{6}$$

The DOS outside the gap can be presented as [21]

$$g_0(p) \approx 0.5c(1-c)N(p)/W(p), \tag{7}$$

where $N(p)$ is the concentration of Mn in $LaMnO_{3+\delta}$ under pressure and $W(p)$ is the bandwidth of the localized electrons depending on p, too. The concentration and the bandwidth parameters are given by the expressions $N(p) = N^*(1+3p/G)$, where $N^* \approx 1.7\times10^{22}$ cm^{-3}, $G = 5\times10^{11}$ N m^{-2} is the Young's modulus [22], and $W(p) \approx W^* T_C(p)/T_C^*$, where from [23] we have $W^* \approx 20kT_C^*/[c(1-c)] \approx 2.2$ eV and 1.0 eV for # 065 and # 154, respectively.

Hence, the experimental values of $\Delta(p)$ in figure 4 can be fitted with equations (5) and (6) using the functions $T_0(p)/T_0^*$, $T_v(p)/T_v^*$, $T_C(p)/T_C^*$ in figure 2, the values given in table 1 and the ratio $a(p)/a^*$ in figure 5 (closed triangles), treating a^* and κ as adjustable parameters. As shown by the solid lines in figure 4, $\Delta(p)$ can be fitted explicitly to the experimental data for both samples, yielding a^* and κ shown in table 1. To obtain continuous curves we used linear

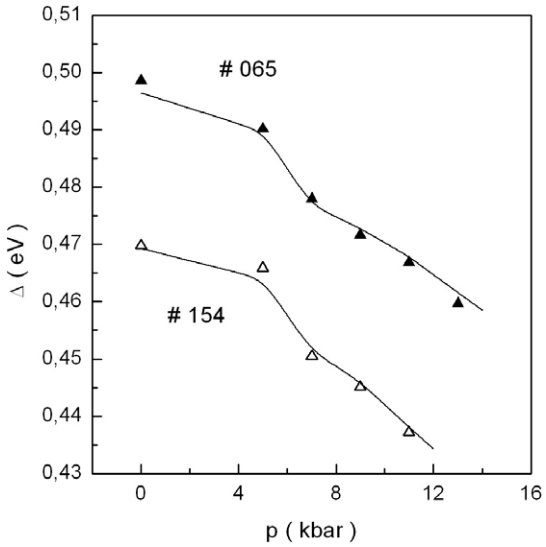

Figure 4. Pressure dependences of the Coulomb gap for # 065 and # 154 (closed and open triangles). The lines are calculated as described in the text.

interpolation of the pressure dependences of the parameters above known only at a discrete pressure values. Finally, with equation (6) we find γ_v^* (see table 1) and the function $\gamma_v(p)/\gamma_v^*$ shown by closed circles in figure 5.

Concerning $\gamma_v(p)$, we also apply the method used for determination of γ_v at ambient pressure in $La_{0.7}Ca_{0.3}Mn_{1-y}Fe_yO_3$ [8], $La_{1-x}Ba_xMnO_3$ [15] and $LaMnO_{3+\delta}$ with $\delta = 0.100$–0.154 [16]. This method is based on analysis of the data of $\rho(T)$ measured in a magnetic field at a given pressure and taking into account the polaronic nature of the charge carriers above T_C. In what follows this will be done for the sample # 065. The localization radius of small polarons in the PM phase is predicted to depend on B as

$$a(B) = a(0)(1 + b_1 B^2), \tag{8}$$

where $b_1 \sim \chi(T)/t$, $\chi(T)$ is the magnetic susceptibility and t is electron transfer integral [23]. For $b_1 B^2 \ll 1$ we obtain from equations (3) and (8)

$$T_0(B) = T_0(0)(1 - b_2 B^2), \tag{9}$$

where $b_2 = b_1 T_{0SE}(0)\{T_0(0) - [T_0(0)/T_v]^{1/2}\gamma_v/(2k)\}^{-1}$ until γ_v is independent of B. This gives

$$\gamma_v = 2\frac{b_1/b_2 - 1}{2b_1/b_2 - 1} k\sqrt{T_0(0)T_v}, \tag{10}$$

where b_1 and b_2 do not depend on T because the temperature dependence of χ is weak near T_v, which is well above T_C, and can be neglected [19]. Therefore, in the vicinity to T_v the dependences of T_0 and A on B at each p can be found from linear fits of the plots of $\ln(\rho/T^{9/2})$ versus $T^{-1/2}$ in the field. The dependence of $a(B)/a$ (0) can be evaluated with equation (2).

As is evident from figure 6, the dependences of $a(B)/a(0)$ and $T_0(B)/T_0(0)$ on B^2 are linear up to $B = 10$ T. The values of b_1 and b_2 are obtained from linear fits of these dependences. For example, in the cases shown in figure 6 we get in units of T^{-2}, $b_1 = (1.54 \pm 0.03) \times 10^{-3}$, $(1.72 \pm 0.05) \times 10^{-3}$ and $(1.82 \pm 0.02) \times 10^{-3}$ and $b_2 = (1.02 \pm 0.01) \times 10^{-3}$, $(1.15 \pm 0.02) \times 10^{-3}$ and $(1.23 \pm 0.01) \times 10^{-3}$ for $p = 1, 9$ and 13 kbar,

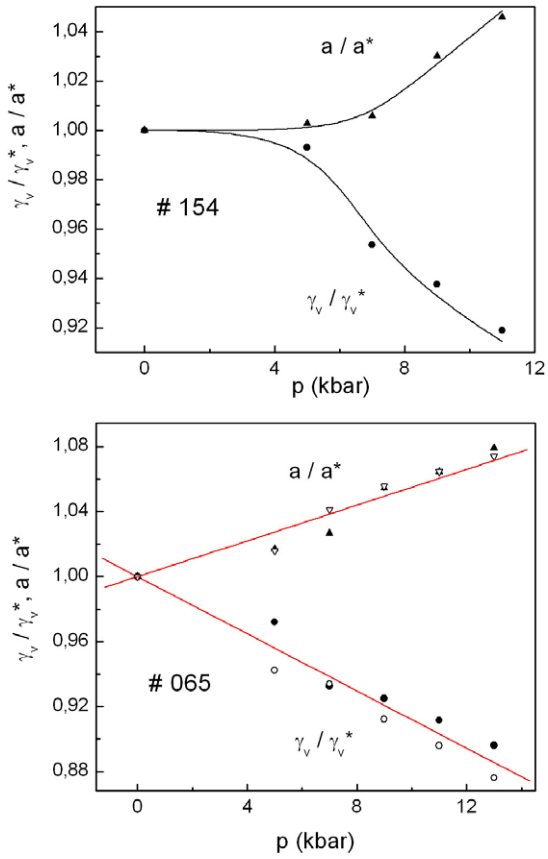

Figure 5. Pressure dependences of a/a^* and γ/γ_v^* for # 154 (top panel) and # 065 (bottom panel). The open and closed symbols in the bottom panel refer to two different methods as described in the text. The lines are to guide the eye.

respectively. It can be seen that the ratio of b_1/b_2 exceeds unity, which means according to equation (10) the existence of a nonzero rigid gap at any p.

Using the values of T_0 and T_v (figure 3 and table 1) with equation (10) we get the same value of γ_v^* as in table 1 and the dependence of $\gamma_v(p)/\gamma_v^*$ shown by open circles in figure 5. With this method the values of $a(p)$ can also be evaluated using equation (6) and the data for $\gamma_v(p)$ obtained with equation (10) and excluding κ from equation (6) with equations (4) and (7). We find $a^* \approx 2.5$ Å, close to that in table 1, and the dependence $a(p)/a^*$ displayed by open triangles in figure 6.

Finally, we analyse the errors of the microscopic parameters above connected to finite intervals ΔT of linearity of the plots in figure 2. Indeed, the linear approximation of any curve contains some arbitrariness when the linear law is expected to be observed only within some limited interval. The model above suggests that T_0 does not depend on T, which is violated as T tends to T_c due to the onset of the temperature dependence of a and γ_v (or, equivalently, deviations from the law $\gamma(T) \approx \gamma_v(T/T_v)^{1/2}$) [8, 15] providing the lower limit of ΔT, whereas its upper limit is connected to the transition to NNH conductivity. Therefore, the satisfactory choice of ΔT means that the variations of the main model parameters, a, γ_v and Δ, in the interval ΔT are small at any p. To check this we assume that all these parameters (as well as

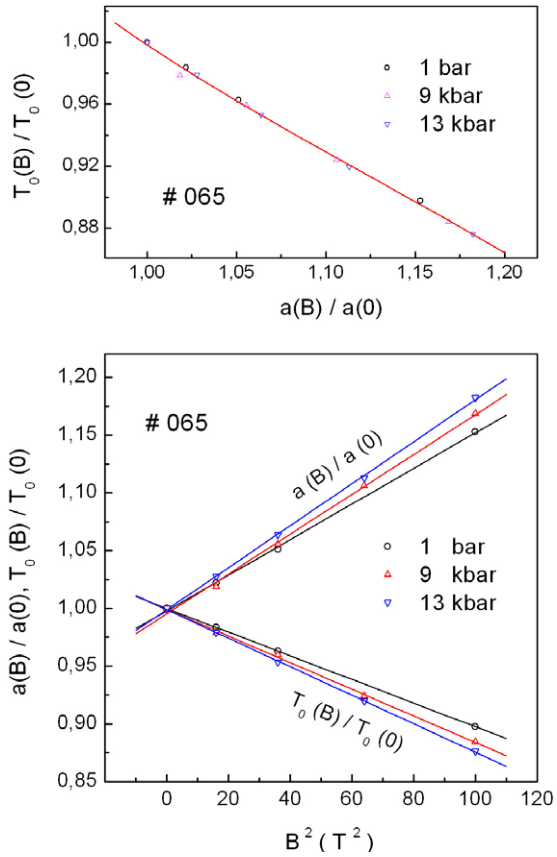

Figure 6. The dependence of $T_0(B)/T_0(0)$ on $a(B)/a(0)$ for # 065. The line is the third-power polynomial fit (top panel). Plots of $a(B)/a(0)$ versus B^2 and $T_0(B)/T_0(0)$ versus B^2 for # 065 under different pressures (bottom panel).

T_0) are functions of T and evaluate them in ΔT with the method proposed in [8] as follows. Let T' be the middle of ΔT; $a' = a(T')$, $\gamma_v' = \gamma_v(T')$, $\Delta' = \Delta(T')$ and $T_0' = T_0(T')$ are the corresponding parameters obtained from the linear approximation of the plots in figure 2 (given in table 1 and figures 3–5). Then from equations (1) and (2) we obtain the first equation,

$$\ln\left[\frac{\rho(T)}{\rho(T')}\left(\frac{T'}{T}\right)^{9/2}\right] = 11\ln\left(\frac{a}{a'}\right) + \frac{7}{2}\ln\left(\frac{T_0}{T_0'}\right) + \left(\frac{T_0}{T}\right)^{1/2} - \left(\frac{T_0'}{T'}\right)^{1/2}, \tag{11}$$

connecting T_0 and a. The second equation can be written in the form

$$T_0/T_0' = f(a/a'), \tag{12}$$

where the function $f(x)$ can be obtained by excluding B from the magnetic field dependences of $T_0(B)/T_0(0)$ and $a(B)/a(0)$ in the bottom panel of figure 6 (this gives a weakly nonlinear function shown in the top panel which can be approximated best with a third- or fourth-order polynomial). The solution of equations (11) and (12) yields $a(T)/a'$ and $T_0(T)/T_0'$; then the functions $\gamma_v(T)/\gamma_v'$ and $\Delta(T)/\Delta'$ can be evaluated with equation (3) and the first of equations (4), respectively, using the data in table 1 and figures 3–5. The final results are presented in figure 7 as the relative variation $\delta a/a' = [a(T) - a']/a'$, $\delta\gamma_v/\gamma_v' = [\gamma_v(T) - \gamma_v']/\gamma_v'$

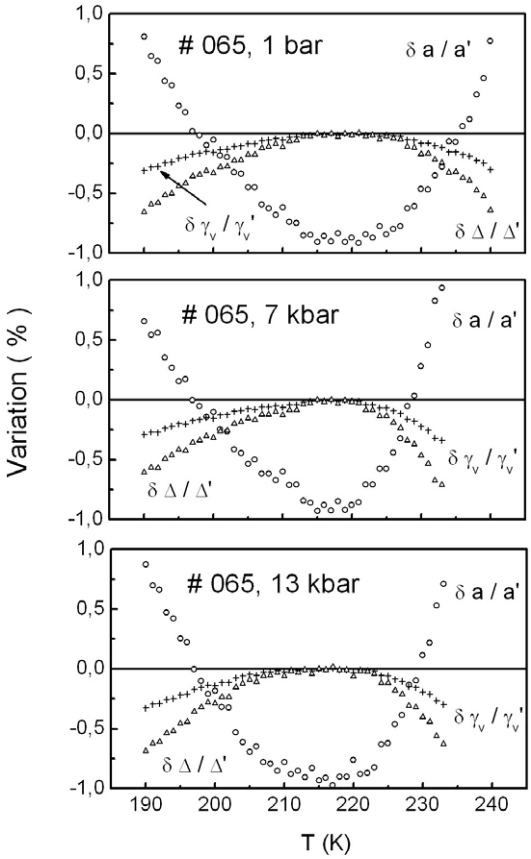

Figure 7. Temperature dependence of the relative variations $\delta a/a'$, $\delta\gamma_v/\gamma_v'$ and $\delta\Delta/\Delta'$ in the intervals ΔT corresponding to linear parts of the plots in figure 2 (bottom panel).

and $\delta\Delta/\Delta' = [\Delta(T) - \Delta']/\Delta'$ of the parameters a, γ_v and Δ, respectively, in the interval ΔT at $p = 1$, 7 and 13 kbar. It can be seen that $\delta a/a' \sim 1\%$, while the others are even smaller, not exceeding typical scattering of the corresponding data points in figures 4 and 5.

4. Discussion

For # 154 the values of a^*, γ_v^* and κ in table 1 are in line with those ($a^* \approx$ 1.7–1.2 Å, $\gamma_v \approx$ 0.13–0.17 eV and $\kappa \approx 3.5$) obtained earlier for $LaMnO_{3+\delta}$ with $\delta = 0.100$–0.154 at ambient pressure [16]. For # 065 the values of κ and a^* are similar to those determined in other manganite perovskites (see section 1), although a^* exceeds that in # 154. The value of γ_v^* in # 065 is the largest among all the CMR materials considered above and exceeds that in # 154 by a factor of almost two. On the other hand, both a^* and γ_v^* and the dependences $a(p)/a^*$ and $\gamma_v(p)/\gamma_v^*$ obtained in # 065 with two different methods are in good agreement (cf the open and the closed symbols in the bottom panel of figure 5).

It can be seen from the inset to the bottom panel in figure 3 that the values of $T_C(p)$ increase with increasing p, following close to a linear function in both samples. In sample # 154 the increase of T_C, with onset of the linear behaviour at $p \sim 4$ kbar, is enhanced. At the same time, both samples demonstrate a negative pressure effect on γ_v (figure 5) which is also

close to linear (in # 154 starting from $p \sim 4$ kbar) and which is stronger in # 065. Finally, the localization radius exhibits approximately a linear increase with p, which is stronger in # 065 and has in # 154 the onset also around $p \sim 4$ kbar.

Generally, in the manganite perovskites the dependence of T_C on pressure is characterized by positive baric coefficients [24]. The values of dT_C/dp and $d(\ln T_C)/dp$ in our $LaMnO_{3+\delta}$ samples (table 1) are similar to those in various other manganite perovskites, lying within the limits of ∼0.9–2.2 K $kbar^{-1}$ and ∼(5–22) $\times 10^{-3}$ $kbar^{-1}$ [24]. In addition, two other features of $T_C(p)$ in figure 3 are in common with those observed in other manganite perovskites: the onset of the linear behaviour is shifted from $p = 0$ (as for # 154) and the pressure effect on T_C is enhanced in compounds with smaller bandwidth (as in # 154 with respect to # 065) [24].

Because $T_C(p) \sim W(p)$ [23, 25], the observed pressure dependence of T_C can be explained by increase of the electron bandwidth due to: (i) *steric effects* or increase of the Mn–O–Mn bond angles and decrease of the corresponding bond lengths increasing the electron transfer integral and the strength of the DE interaction, and (ii) *polaronic effects* or polarization of the lattice and surrounding Mn spins of the charge carriers [2, 20]. On the other hand, according to the origin of the rigid gap supposed above (see section 1) we can write $\gamma_v = E_p/2 - E_d/2$ [15], where E_p is the depth of the polaron potential well due to local lattice distortions and spin polarization and E_d is the width of the electron potential energy distribution due to lattice and spin disorder [15].

The smaller bandwidth in # 154 is connected to its strongly distorted rhombohedral crystal structure, whereas the larger value of W for # 065 is due to only small rhombohedral distortions of cubic structure [19]. On the other hand, the larger value of γ_v in # 065 suggests stronger polaron effects in this sample with respect to # 154, because the degree of disorder in $LaMnO_{3+\delta}$ is small [19]. Therefore, it is likely that reason (i) dominates the pressure effect on T_C in # 154 having more possibilities to increase the Mn–O–Mn bond angles under pressure. Reason (ii) should prevail in the pressure dependence of T_C in # 065 having an advantage of decreasing depth of the polaron potential well when p is increased. This can explain the enhanced pressure effect on T_C in # 154 and simultaneously the stronger pressure dependence of γ_v in # 065.

The degree of localization of the charge carriers in the manganites is governed by the electron bandwidth and the depth of the polaron potential well. Because $E_d \ll E_p$, the value of $E_p \approx 2\gamma_v$ in # 065 exceeds that in # 154 by a factor of approximately two, which should lead to a smaller value of a^*, but only if these samples have the same W. However, the bandwidth in # 065 is more than twice as large as that in # 154, resulting in larger a^*. As follows from the discussion above, W increases under pressure whereas E_p decreases, both tending towards delocalization of the electrons and increasing the value of $a(p)$ (figure 5).

5. Conclusions

We have investigated the resistivity of $LaMnO_{3+\delta}$ under pressure. Shklovskii–Efros-like variable-range hopping conductivity, governed by the soft Coulomb gap and the rigid gap, attributable to the polaronic nature of the charge carriers, is observed between the onset temperature T_v and the Curie temperature T_C. The pressure dependences of the macroscopic parameters, including T_v, the characteristic VRH temperature T_0, T_C and the prefactor constant A, as well as the pressure effect on the microscopic parameters such as the widths of the soft and the rigid gaps and the localization radius, are obtained. These dependences can be attributed to increasing of the electron bandwidth and decreasing of the depths of the polaron potential well under pressure, both tending towards delocalization of the charge carriers. The first of these reasons, with prevailing steric effects, is more pronounced in the sample with larger δ

(0.154) and strongly distorted rhombohedral crystal structure, while the second one, related to polaronic effects, dominates in the material having smaller δ (0.065) and weakly distorted cubic structure but a deeper polaron potential well.

References

[1] Von Helmolt R, Wecker J, Holzapfel B, Schulz L and Sammer K 1993 *Phys. Rev. Lett.* **71** 2331
Schiffer P, Ramirez A P, Bao W and Cheong S-W 1995 *Phys. Rev. Lett.* **75** 3336
[2] Tokura Y (ed) 2000 *Colossal Magnetoresistive Oxides* (Amsterdam: Gordon and Breach)
[3] de Gennes P-G 1960 *Phys. Rev.* **118** 141
[4] Töpfer J and Goodenough J B 1997 *J. Solid State Chem.* **130** 117
[5] Millis A J, Littlewood P B and Shraiman B I 1995 *Phys. Rev. Lett.* **74** 5144
[6] Worledge D C, Snyder G J, Beasley M R and Geballe T H 1996 *J. Appl. Phys.* **80** 5158
[7] Shklovskii B I and Efros A L 1984 *Electronic Properties of Doped Semiconductors* (Berlin: Springer)
[8] Laiho R, Lisunov K G, Lähderanta E, Petrenko P A, Salminen J, Shakhov M A, Safontchik M O, Stamov V S, Shubnikov M V and Zakhvalinskii V S 2002 *J. Phys.: Condens. Matter* **14** 80439
[9] Biswas A, Elizabeth S, Raychaudhuri A K and Bhat H L 1999 *Phys. Rev.* B **59** 5368
[10] Kim K W, Lee J S, Noh T W, Lee S R and Char K 2005 *Phys. Rev.* B **71** 125104
[11] Yakimov A I, Wright T, Adkins C J and Dvurechenskii A V 1995 *Phys. Rev.* B **51** 16549
[12] Kim J J and Lee H J 1993 *Phys. Rev. Lett.* **70** 2798
[13] Terry I, Penny T and von Molnar S 1992 *Phys. Rev. Lett.* **69** 1800
[14] Lisunov K G, Arushanov E, Vinzelberg H, Behr G and Schumann J 2005 *J. Appl. Phys.* **97** 093706
[15] Laiho R, Lisunov K G, Lähderanta E, Shakhov M A, Stamov V N, Zakhvalinskii V S, Kozhevnikov V L, Leonidov I A, Mitberg E B and Patrakeev M V 2005 *J. Phys.: Condens. Matter* **17** 3429
[16] Laiho R, Lisunov K G, Lähderanta E, Stamov V S, Zakhvalinskii V S, Colomban Ph, Petrenko P A and Stepanov Yu P 2005 *J. Phys.: Condens. Matter* **17** 105
[17] Mott N F and Davies EA 1979 *Electron Processes in Non-Crystalline Materials* (Oxford: Clarendon)
Mott N F 1990 *Metal–Insulator Transitions* (London: Taylor and Francis)
[18] Alexandrov A S and Bratkovsky A M 2000 *J. Appl. Phys.* **87** 5016
[19] Laiho R, Lisunov K G, Lähderanta E, Petrenko P A, Salminen J, Stamov V N, Stepanov Yu P and Zakhvalinskii V S 2003 *J. Phys. Chem. Solids* **64** 2313
[20] Vazques-Vazques C, Carmen Blanco M, Arturo Lopez-Quintela M, Sanchez R D, Rivas J, Saul N and Oseroff B 1998 *J. Mater. Chem.* **8** 991
[21] Viret M, Ranno L and Coey J M D 1997 *Phys. Rev.* B **55** 8067
[22] Moshnyaga V, Klimm S, Gommert E, Tidecks R, Hom S and Samwer K 2000 *J. Appl. Phys.* **88** 5305
[23] Varma C M 1996 *Phys. Rev.* B **54** 7328
[24] Laukhin V, Fontcuberta J, Garcia-Munoz J L and Obrados X 1997 *Phys. Rev.* B **56** R10009
[25] Garcia-Munoz J L, Fontcuberta J, Suaadi M and Obrados X 1996 *J. Phys.: Condens. Matter* **8** L787